JOURNAL OF SPACECRAFT AND ROCKETS
Vol. 36, No. 6, November–December 1999

Engineering Notes

ENGINEERING NOTES are short manuscripts describing new developments or important results of a preliminary nature. These Notes cannot exceed 6 manuscript pages and 3 figures; a page of text may be substituted for a figure and vice versa. After informal review by the editors, they may be published within a few months of the date of receipt. Style requirements are the same as for regular contributions (see inside back cover).

Aerothermodynamic Analyses of Hypersonic, Blunt-Body Flows

Henry A. Carlson*
Raytheon Missile Systems Company,
Tucson, Arizona 85734-1337

Nomenclature

a = speed of sound, m/s
c = mass fraction
Da_c = chemical Damköhler number
Da_v = vibrational Damköhler number
E_a = Arrhenius activation energy, W/kg
K_{eq} = equilibrium constant
Kn = Knudsen number
k_f = forward reaction rate coefficient
L = computational cell length, m
l_f = flow length scale, normalized by hemisphere radius
M = molecular weight, kg/kmol
Ma = Mach number
p = static pressure, Pa
q = surface heat flux, W/m^2
R = gas constant, W/kgK
Re = Reynolds number
Re_{cell} = cell Reynolds number
T = translational/rotational temperature, K
T_v = vibrational temperature, K
t = time, s
$t_{c,f,v}$ = chemical, flow, and vibrational time scales, s
u = velocity, m/s
x = streamwise distance, m
$\tilde{x}$ = streamwise distance, normalized by hemisphere radius
α'_{ij} = stoichiometric coefficient of reactant i in reaction j
α''_{ij} = stoichiometric coefficient of product i in reaction j
ν = kinematic viscosity, m^2/s
ρ = mixture density, kg/m^3

I. Introduction

AEROTHERMODYNAMIC analyses play a critical role in designing a vehicle for hypersonic flight. In these flow regimes, aerothermal contributions to the overall thermal load are zeroth order and may have a major impact on the structural integrity of the vehicle. In the case of a sensor-guided weapon system, the thermostructural effects upon sensor performance may be significant—tilting and defocus of the mirror in an optical assembly because of the thermal growth of support struts, for instance.

Obtaining accurate heat-transfer rates in a hypersonic shock tunnel can be difficult, given the short available test times and high temperatures, and expensive, particularly for complex vehicle geometries. The engineer must often rely on computational methods in determining hypersonic aerothermal loads. Computational codes can be validated, in an indirect manner, by comparing simulation results and experimental data at matching conditions but with simpler geometries. To this end, comparisons are made with heating data obtained in tests performed in the Calspan 96-in. hypersonic shock tunnel.[1] In Sec. II, these experimental data are compared with computational fluid dynamics (CFD) solutions from LAURA[2] and GASP,[3] a direct simulation Monte Carlo (DSMC) solution from G2 (Ref. 4), and the semi-empirical solutions of Fay and Riddell.[5]

Section III consists of an analysis of the chemical composition and vibrational-mode energy levels of the flow and the impact of computational modeling options on the results. Again, motivation for the investigation derives from the potential effects on vehicle sensor performance. Absorption and scattering of the optical signal in critical wavebands and emission of signal background noise (photons) within the sensor field of view are functions of the degree of chemical dissociation and the level of vibrational excitation in the shock layer. The goal is a means of 1) estimating the thermochemical properties of a flow, 2) anticipating the relevant physics, and 3) guiding the modeling choices that are made before a computational analysis begins.

II. Comparisons of Aerothermal Data

The freestream conditions and the experimentally measured stagnation point pressures and heat fluxes of the five Calspan runs are listed in Table 1. Reynolds and Knudsen numbers are based on the radius of the hemisphere. The altitudes at which atmospheric densities match the freestream densities are included in this table. The aerothermal comparisons are summarized in Table 2: percentage differences between the computational/semi-empirical values of stagnation-point heat flux and the experimental values for each of the Calspan runs. Because of time and computational resource constraints, simulations using all of the codes and all of the various thermochemical models were not performed for each test point. However, enough data were gathered to establish a range of uncertainty.

All but one of the computational values are higher than the corresponding experimental value in runs 892 (both diameters), 896 (0.50-in. diameter), and 1283. In these cases, the uncertainty is approximately 27%. The reverse is true for the 3.00-in.-diam hemisphere in run 896: all but one of the computational predictions are lower than the experimental value. Here, uncertainty in the computational results is approximately 20%, and all three Fay–Riddell[5] predictions lie below the experimental value. The percentage differences between perfect gas Fay–Riddell predictions and experimental values, as reported by Chadwick,[1] are approximately equal to those listed in Table 2 in all cases except run 892 (0.5-in. diam) where the difference was reported as zero. All of the computational and analytical values of stagnation pressure lie within 5% of the corresponding experimental value (for all of the test cases). The relatively narrow range of uncertainty is to be expected because pressure is a function of the inviscid model only and not of viscous, boundary-layer effects.

In the semi-empirical formulations for perfect gas and frozen flows, thermodynamic properties at the boundary-edge are calculated from the one-dimensional equations for conditions across a normal shock.[6,7] In the case of equilbrium air, the conditions are computed iteratively from equilibrium equations of state. Total

Received 6 July 1998; revision received 18 May 1999; accepted for publication 18 May 1999.

*Senior Engineering Specialist, Mechanical Airframe Design and Analysis Center, Raytheon Systems Co., 100 Graham Road, Unit 9C, Ithaca, NY 14850-1105. Member AIAA.

Table 1 Freestream conditions and stagnation point values of the Calspan runs

Run	Diameter, in.	u_∞, km/s	ρ_∞, kg/m^3	Altitude, km	T_∞, K	Ma_∞	Re_∞	Kn_∞	p_s, Pa	q_s, W/m^3
892	0.50	3.566	8.452e−4	51.5	167.8	13.71	1.678e+3	1.145e−2	9.860e+3	2.912e+6
892	3.00	3.566	8.452e−4	51.5	167.8	13.71	1.007e+4	1.908e−3	9.860e+3	1.247e+6
896	0.50	2.300	3.490e−2	25.9	138.8	9.749	5.348e+4	2.772e−4	1.703e+5	3.998e+6
896	3.00	2.300	3.490e−2	25.9	138.8	9.749	3.209e+5	4.620e−5	1.703e+5	2.489e+6
1283	1.25	2.296	1.728e−4	64.0	55.15	15.40	1.742e+3	2.240e−2	8.260e+2	1.748e+5

Table 2 Percentage differences between the computational/analytical values of stagnation-point heating and the experimental value for each of the Calspan runs

		Calspan run				
		892		896		1283
		Diameter		Diameter		Diameter,
Code	Mode[a]	0.50	3.00	0.50	3.00	1.25
LAURA	1	+9.11	+2.21	+23.54	−9.05	+20.81
	2	+24.12	+0.11	+25.83	−7.61	+25.33
	3	+16.35	−1.46	+23.76	−7.65	+25.12
	4	+17.00	+5.81	+24.58	−8.02	+25.12
	5	+18.01	+2.57			+25.31
GASP	1	+21.00	+13.08		+11.03	
	2	+7.92	+0.51			
	3	+8.09	+3.92			
G2 (DSMC)	6					+33.51
Fay–Riddell[5]	1	−3.06	−7.60	+11.21	−27.07	+8.54
	2	+3.29	−1.54	+19.64	−21.54	+15.84
	7	−35.05	−38.09	+18.56	−22.24	+10.01

[a]The models are 1) perfect gas, 2) equilibrium air, 3) chemical nonequilibrium with a noncatalytic wall, 4) chemical nonequilibrium with an equalibrium-catalytic wall, 5) chemical and vibrational nonequilibrium with a noncatalytic wall, 6) single species, and 7) chemically frozen with a noncatalytic wall.

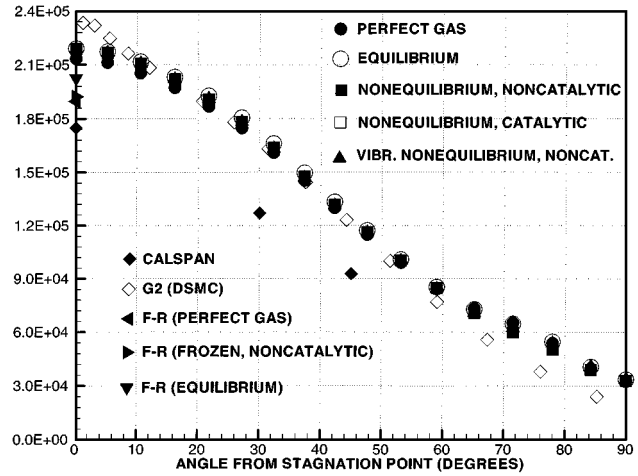

Fig. 1 Calspan run 1283, 1.25-in.-diam hemisphere: surface heat fluxes in W/m^2 from LAURA and comparisons with values from Calspan, G2, and Fay and Riddell[5] (F–R).

stagnation-point enthalpy is calculated by integrating along a streamline from the boundary-layer edge. A Lewis number of unity is used in the Fay–Riddell calculations. (Stagnation heating values would be approximately 8% higher if the assigned Lewis number was 1.4.)

In the CFD simulations, the computational domains are three dimensional, consisting of o-grid topologies. The number of grid points in the wall-normal direction is 65 and in both circumferential directions 33. LAURA has the capability of automatically adapting the computational grid to capture the bow shock and to refine the boundary layer. The controlling parameter in the wall region is the cell Reynolds number ($Re_{\text{cell}} = aL/\nu$). From the molecular definitions of the speed of sound and kinematic viscosity, $a/\nu \approx \lambda^{-1}$, so that a cell with a Reynolds number of one has a dimension of one mean free path. In each of the final LAURA solutions, the specified cell Reynolds number is 0.5. To maintain consistent spatial resolution of the boundary layers, adapted grids from LAURA are used with GASP.

In the nonequilibrium modes of both GASP and LAURA, five species (N_2, O_2, N, O, and NO) and finite reaction rates are modeled. The vibrational nonequilibrium mode consists of a two-temperature model that does not include preferential dissociation of vibrationally excited molecules.[8] In the equilibrium-catalytic wall mode, surface mass fractions are defined by the equilibrium composition at the given wall temperature. In the noncatalytic mode, the fluid is chemically frozen at the wall.

Figure 1 contains plots from LAURA of surface heat flux for run 1283 (1.25-in.-diam hemisphere). In this case, three experimental data points are available at angles of 0, 30, and 45 deg. The highest stagnation-point flux is predicted in the DSMC simulation. Even though the conditions of run 1283 are the most rarefied in the database, the Knudsen number falls well within the range for continuum flow. The DSMC chemistry model consists of a single, diatomic species—chemical reactions are not modeled; vibrational nonequilibrium is. Although underresolution at the wall can result in overprediction of heat flux in a DSMC simulation, the value of L/λ at the stagnation point is less than 1.0 in the G2 run, and the boundary layer should be adequately resolved.

In a grid resolution study, data were compared from LAURA simulations on coarse and fine grids corresponding to prescribed cell Reynolds numbers of 10 and 0.5. With these target values, the automatic grid adaption algorithm produces cells at the wall with values of L/λ that differ by a factor of approximately 10. The fine grids produced 5, 8, and 5% higher stagnation heating values for Calspan runs 892 (0.5-in. diameter, perfect gas), 896 (3.00-in. diameter, perfect gas), and 896 (3.00-in. diam, equilibrium air), respectively. Again, the fluxes in Table 2 correspond to solutions on fine grids where the cell Reynolds numbers are 0.5.

III. Chemical Activity and Vibrational Mode Excitation

Even when the influence on aeroheating is small, the levels of chemical and vibrational nonequilibrium in the field of view of a sensor can be important because of photon emission and signal absorption/scattering. Code limitations and computer resource constraints often force one to choose the perfect gas model over something more sophisticated. Comparing the equilibrium and nonequilibrium solutions for run 892 (3.00-in. diam), the maximum temperature in the shock is 60% lower when chemical equilibrium is assumed (3200 vs 5131 K). The maximum mass fraction of monotonic oxygen in the shock and boundary layers—assuming equilibrium—is approximately one order of magnitude higher (1.45×10^{-1} vs 1.71×10^{-2}). Complete dissociation of diatomic oxygen would yield an O mass fraction of 2.32×10^{-1}. A maximum temperature of 6262 K and maximum O_2 mass fraction of 2.32×10^{-1} (from the perfect gas simulation) may be exceedingly conservative from the standpoint of the effect on sensor performance.

Another consideration is the level of vibrational mode excitation. From the vibrational nonequilibrium simulation for run 892 (3.00-in. diameter), vibrational mode excitation is lower than translational throughout most of the domain, which attenuates the dissociation process. The maximum mass fraction of O is 1.36×10^{-2}, compared to 2.55×10^{-2} in the vibrational equilibrium simulation. Run 892 is the test point with the highest enthalpy, and the

3.00-in.-diam case has the highest level of oxygen dissociation. Run 1283 (1.25-in. diam), the most rarefied test condition, has the least amount of dissociated oxygen—almost none. Yet, of the five test points, it has the highest degree of vibrational nonequilibrium: The ratio of vibrational to translational temperature is 2% in a relatively broad region that extends from the outer edge of the shock layer to well within the boundary layer.

Several nondimensional parameters reflect the potential level of chemical activity and the degree of chemical and vibrational nonequilibrium in a flow. The inverse of the Zel'dovich number is a measure of whether a flow has the energy required for chemical reactions[9]: $Ze^{-1} = RT/E_a$. In the flows considered here, the activation energy corresponds to O_2, and $Ze^{-1} \gg 1$ indicates that dissociation will occur where the gas has equilibrated chemically. The chemical Damköhler number ($Da_c = t_f/t_c$) is a measure of the degree of equilibrium.[10] For $Da_c \gg 1$, the flow is in chemical equilibrium, and for $Da_c \ll 1$ the flow is chemically frozen. The local timescale of the flow is $t_f = \rho/(u|\nabla\rho|)$. The chemical timescale of species i is a function of its production rate, $t_c = \rho_i(\partial\rho_i/\partial t)^{-1}$, where the production rate is determined from the reactions involving the species. Forward reaction rates are functions of temperature and are computed from the Arrhenius equation with coefficients from Park.[11] For dissociation of oxygen via collisions with diatomic nitrogen ($O_2 + N_2 \rightarrow 2O + N_2$), the production rate of monatomic oxygen is

$$\frac{\partial\rho_O}{\partial t} = 2M_O k_f \left[\frac{\rho_{O_2}}{M_{O_2}} \frac{\rho_{N_2}}{M_{N_2}} - K_{eq}^{-1} \frac{\rho_{N_2}}{M_{N_2}} \left(\frac{\rho_O}{M_O} \right)^2 \right] \qquad (1)$$

Local values of Ze^{-1} and Da_c have been computed from the CFD solutions and are plotted along with the mass fraction of O and the local length scale of the flow ($l_f = \rho/|\nabla\rho|$) in Figs. 2 and 3. The independent variable is the normalized distance from the stagnation point ($\tilde{x}$), along a line that is collinear to the freestream velocity vector. Along this line, changes in the flow properties are most pronounced, gradients steepest. All lengths are normalized by the radii of the hemispheres. The flow direction is from the outer edge of the shock layer on the far left to the stagnation point on the far right. The data of Figs. 2 and 3 are from LAURA solutions, using the chemical nonequilibrium model.

By its definition, the local length scale approaches infinity in the freestream. Small values of l_f delineate the shock and boundary layers. From Fig. 2 (run 892, 3.00-in. diameter), the shock layer extends from $\tilde{x} = 0.11$ to 0.09 and the boundary layer from $\tilde{x} = 0.03$ to 0.00. Figure 3 indicates a wider shock layer for the 0.50-in. hemisphere—from approximately $\tilde{x} = 0.13$ to 0.09—and a much smaller separation between the shock and boundary layers. The normalized locations of the shock centers are approximately the same. The mass fraction of O at the wall is nonzero in both cases, reflecting noncatalytic boundary conditions. There is an order of magnitude difference between the maximum mass fractions of O, with the larger body engendering significantly more dissociation.

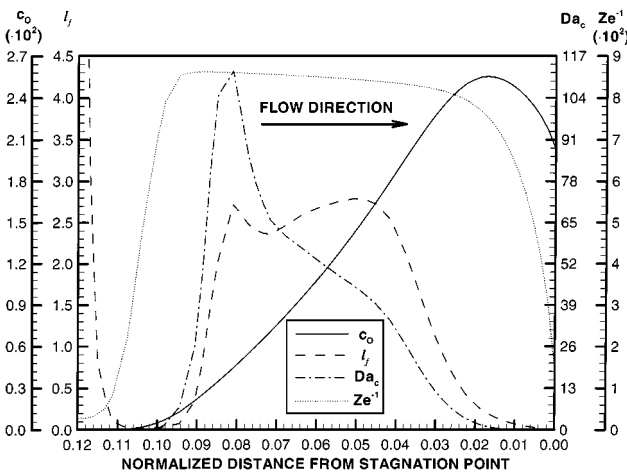

Fig. 2 Calspan run 892, 3.00-in.-diam hemisphere: one-dimensional plots of c_O, l_f, Da_c, and Ze^{-1}.

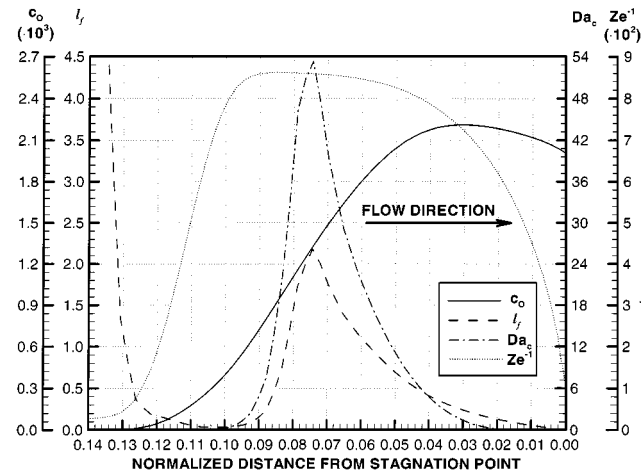

Fig. 3 Calspan run 892, 0.50-in.-diam hemisphere: one-dimensional plots of c_O, l_f, Da_c, and Ze^{-1}.

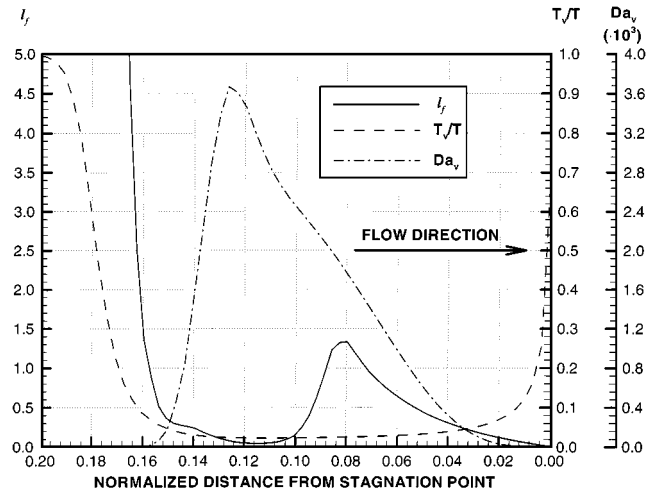

Fig. 4 Calspan run 1283, 1.25-in.-diam hemisphere: one-dimensional plots of l_f, T/T_v, and Da_v.

The Zel'dovich number maxima are roughly equal, although the highest values extend about twice as far for the larger body, through the larger region that separates the shock and the boundary layers. The primary difference between the two flows appears to be the degree of chemical equilibrium, as reflected in Da_c, which has a peak value of 115 for the larger body and 54 for the smaller.

The vibration Damköhler number is a measure of the degree of vibrational nonequilibrium: $Da_v = t_f/t_v$. For $Da_v \gg 1$, the flow is in vibrational equilibrium, and for $Da_v \ll 1$ the flow is frozen vibrationally. The characteristic vibrational relaxation time of a species is a function of its characteristic temperature of vibration and its reduced mass.[12] Values of Da_v have been computed from the LAURA solutions that employ the vibrational and chemical nonequilibrium model. Because almost 80% of the gas mixture is composed of diatomic nitrogen, N_2 is the chosen species. Local values of l_f, T_v/T (the ratio of vibrational to translational temperature), and Da_c are plotted in Fig. 4 for run 1283, the test point with the highest levels of vibrational nonequilibrium. From the values of l_f, the shock layer extends approximately from $\tilde{x} = 0.15$ to 0.10. As was the case with the smaller diameter hemisphere of run 892, the distance separating the shock and boundary layers is small.

The region of vibrational nonequilibrium, where T_v/T is low, begins at the outer edge of the shock and extends through most of the boundary layer. The peak value of Da_v that occurs at the center of the shock layer may be misleading. First, t_v increases as the

Table 3 Comparison of the maximum computed values of the nondimensional parameters and estimated values using conditions behind a normal shock

		Maximum computed values				Estimated values			
Calspan run	Diameter, in.	c_O	Ze^{-1}	Da_c	Da_v	c_O	Ze^{-1}	Da_c	Da_v
892	3.00	2.5e−2	8.6e−2	1.1e+2	5.6e+1	1.7e−1	1.0e−1	1.4e−1	2.4e+0
892	0.50	2.2e−3	8.6e−2	5.3e+1	1.4e+1	7.6e−2	1.0e−1	2.4e−2	4.1e−1
896	3.00	2.7e−5	4.0e−2	3.1e+3	2.6e+2	3.1e−4	4.5e−2	6.5e−5	1.3e+0
896	0.50	2.2e−8	4.0e−2	1.2e+6	1.9e+0	5.1e−5	4.5e−2	1.1e−5	2.2e−1
1283	1.25	8.3e−9	3.8e−2	4.5e+2	3.7e−3	0.0e+0	4.4e−2	6.7e−8	2.3e−3

translational temperature decreases, becoming quite large as temperatures approach the values at the wall and very large as they approach freestream values. Even though t_f approaches infinity in the freestream, t_c approaches infinity faster, and this accounts for the low values of Da_v outside the shock where the flow is actually in vibrational equilibrium. Close to the wall, t_f approaches zero faster than t_c, and this drives down the value of Da_v. The salient point is that the maximum value of Da_v is relatively low in run 1283, reflecting a relatively high degree of vibrational nonequilibrium.

Table 3 provides a summary of the maximum computed values of c_O, Ze^{-1}, Da_c, and Da_v from the LAURA solutions. These are compared with estimated values of Ze^{-1}, Da_c, and Da_v, obtained from the definitions using values of temperature, pressure, density, and velocity calculated from freestream conditions and the perfect gas relations for flow across a one-dimensional, normal shock. In estimating t_f, the length scale of the flow is taken to be equal to the radius of the hemisphere. In addition, the mass fraction of monatomic oxygen is estimated from the equation for the chemical Damköhler number. The sum of the mass fractions of O_2 and O is a constant, yielding a quadratic equation for c_O:

$$Ac_O^2 + Bc_O + C = 0 \tag{2}$$

$$A = \frac{\rho M_{O_2}}{K_{eq} M_O^2}, \qquad B = 1 + \frac{M_{O_2} M_{N_2} Da_c}{2\rho M_O k_f c_{N_2} t_f}, \qquad C = c_{N_2} - 1 \tag{3}$$

Using the conditions behind a normal shock and assuming a Damköhler number of 1.0, one root of the quadratic equation is negative and is discarded. The positive root is taken as an estimate of the level of oxygen dissociation. Choice of the value of Da_c is arbitrary; the goal is an estimate of relative, not absolute, levels of chemical activity. The entries of Table 3 are listed in order of decreasing amounts of oxygen dissociation. The orderings of estimated values of c_O and maximum computed values match, despite significant absolute differences. The same is true of the nondimensional parameters. As is borne out in the simulations, run 1283 has the lowest level of chemical activity and the highest degree of vibrational nonequilibrium, indicated by the lowest values of Da_c and Da_v.

Given problems involving more complicated, computationally expensive geometries, these estimates may provide guidance in the selection of thermochemical models. The CPU time required for a simulation with multiple species, each in vibrational nonequilibrium, can be an order of magnitude greater than that required for a perfect gas simulation. Moreover, finite reaction rate models can produce stiff governing equations, resulting in major convergence problems.[13] These are compelling reasons for avoiding a model that is more complex than the physics of the flow.

IV. Conclusions

Comparisons of experimental, computational, and semi-empirical values of stagnation pressure and heat flux on blunt bodies in hypersonic flows indicate approximate ranges of uncertainty of 5 and 25%, respectively. Two CFD codes (LAURA and GASP) and one DSMC code (G2) were tested. In the cases examined, neither the thermochemical model nor the surface catalysis model has a major influence on the computational aeroheating results—for obvious reasons in the cases where chemical activity is negligible and because of recombination in the boundary layer for the others. Although experimental data are not available for comparison, computational predictions of the flow properties in the shock and boundary layers have been examined.

Local values of the inverse of the Zel'dovich number, the chemical Damköhler number, and the vibrational Damköhler number, computed from each CFD solution, distinguish the chemical potential and the nonequilibrium effects that characterize a flow. Estimates of these nondimensional parameters using freestream conditions, body size, and one-dimensional, normal shock relations provide accurate, relative predictions of levels of dissociation and nonequilibrium and may be used as guides in the selection of the computational model.

Acknowledgments

The author thanks K. M. Chadwick of Calspan SRL Corporation for providing the experimental data; P. A. Gnoffo of NASA Langley Research Center for help with LAURA and assistance with data interpretation; D. C. Slack and W. M. Eppard of AeroSoft, Inc., for help with GASP; and H. H. Hamilton of NASA Langley Research Center for providing the semi-empirical, stagnation heating formulations.

References

[1]Chadwick, K. M., "Stagnation Heat Transfer Measurement Techniques in Hypersonic Shock Tunnel Flows over Spherical Segments," AIAA Paper 97-2493, June 1997.

[2]Cheatwood, F. M., and Gnoffo, P. A., "User's Manual for the Langley Aerothermodynamic Upwind Relaxation Algorithm (LAURA)," NASA TM 4674, April 1996.

[3]Walters, R. W., Applebaum, M. P., Eppard, W. M., Fury, C. B., Godfrey, A. G., McGrory, W. D., and Slack, D. C., *General Aerodynamic Simulation Program Version 3 Users Manual*, Aerosoft, Inc., Blacksburg, VA, May 1996.

[4]Bird, G. A., "Axially Symmetric Flows," *Molecular Gas Dynamics and the Direct Simulation of Gas Flows*, Clarendon, Oxford, 1994, pp. 370–388.

[5]Fay, J. A., and Riddell, F. R., "Theory of Stagnation Point Heat Transfer in Dissociated Air," *Journal of the Aeronautical Sciences*, Vol. 25, No. 2, 1958, pp. 73–85, 121.

[6]Hamilton, H. H., "Approximate Method of Calculating Heating Rates at General Three-Dimensional Stagnation Points During Atmospheric Entry," NASA TM 84580, Nov. 1982.

[7]Hansen, C. F., "Approximations for the Thermodynamic and Transport Properties of High-Temperature Air," NACA TN 4150, March 1958.

[8]Park, C., "Two-Temperature Interpretation of Dissociation Rate Data for N_2 and O_2," AIAA Paper 88-0458, Jan. 1988.

[9]Bruno, C., "Real Gas Effects," *Hypersonics 1*, Birkhauser, Boston, 1989, pp. 303–354.

[10]Penner, S. S., "Similarity Analysis for Chemical Reactors and the Scaling of Liquid Fuel Rocket Engines," *Combustion Researches and Reviews*, Butterworths Scientific, London, 1955, pp. 140–162.

[11]Park, C., "Calculation of Nonequilibrium Radiation in AOTV Flight Regimes," AIAA Paper 84-0306, Jan. 1984.

[12]Millikan, R. C., and White, D. R., "Systematics of Vibrational Relaxation," *Journal of Chemical Physics*, Vol. 39, No. 12, 1963, pp. 3209–3213.

[13]Park, C., "On Convergence of Computation of Chemically Reacting Flow," AIAA Paper 85-0247, Jan. 1985.

B. A. Bhutta
Associate Editor